Observed Interaction between Pacific Sea Ice and the Western Pacific Pattern on Intraseasonal Time Scales

N. JOSS MATTHEWMAN AND GUDRUN MAGNUSDOTTIR

Department of Earth System Science, University of California, Irvine, Irvine, California

(Manuscript received 22 November 2010, in final form 12 March 2011)

ABSTRACT

The relationship between North Pacific sea ice and the Western Pacific (WP) pattern is examined using wintertime observational data between 1978 and 2008. Weekly averaged data are chosen to capture the characteristically short time scale of the WP. A clear relationship is found between the WP and sea ice concentrations in the Bering Sea, where the positive polarity of the WP is accompanied by increasing sea ice concentrations and the negative WP by decreasing sea ice concentrations. Sea ice concentrations in the Sea of Okhotsk, however, are shown to be largely insensitive to the strength of the WP. Feedback of Bering Sea sea ice concentrations onto the WP is tested by fitting weekly averaged observations to a vector autoregressive (VAR) model. Results from the VAR model indicate that feedback of Bering Sea sea ice onto the WP plays a significant role in the dynamics of the WP and that this feedback is positive; that is, WP-induced changes in Bering Sea sea ice concentrations help sustain existing WP conditions, thereby lengthening the time scale of variability of the WP.

1. Introduction

One of the dominant modes of atmospheric variability controlling regional climate in the Pacific sector is the Western Pacific (WP) pattern. The WP signal is observed in midtropospheric (500 hPa) geopotential height fields and is characterized by a trough over Alaska and the Bering Strait, and peaks over the central Pacific and North America south of Hudson Bay (Wallace and Gutzler 1981; Nigam 2003). This mode of variability has important implications for North American climate, being linked to increased precipitation along the Alaskan and Canadian coasts and over the south-central Great Plains (Linkin and Nigam 2008). The WP is largely equivalent barotropic and can be considered as the midtropospheric manifestation of the North Pacific Oscillation (NPO) in sea level pressure (Walker and Bliss 1932; Rogers 1981); that is, the two patterns can be treated as different faces of the same phenomenon (Linkin and Nigam 2008). Geopotential height anomalies associated with the WP pattern have a characteristically short time scale of approximately 7.4 days, slightly shorter than the 9.5-day time scale of its Atlantic sector counterpart, the North Atlantic Oscillation (NAO) (Feldstein 2000).

Sea ice variability in the Pacific sector is primarily confined to the Bering Sea and Sea of Okhotsk, with the leading mode appearing as a dipole in sea ice concentration between seas (Cavalieri and Parkinson 1987; Fang and Wallace 1994; Liu et al. 2007; Ukita et al. 2007). However, using winter mean data, Liu et al. (2007) noted that sea ice concentration anomalies between seas are in phase just as often as out of phase, indicating that dynamical interactions governing growth and decay of sea ice may differ between the two, supporting an approach in which each sea is treated independently, rather than as a dipole pair. Several mechanisms link variability in the atmosphere, such as that associated with the WP, with this variability in Pacific sea ice. Atmospheric forcing of sea ice can occur via wind-forced changes in oceanic heat transport assisting or inhibiting sea ice melt, and sea ice advection by surface winds. In return, sea ice exerts influence on the overlying atmosphere via surface flux of sensible and latent heat, which depends sensitively on sea ice concentration. For example, variations in total heat flux are of order 250 W m^{-2} in the marginal sea ice zone in the

Corresponding author address: Nicolas Joss Matthewman, Dept. of Earth System Science, University of California, Irvine, Irvine, CA 92697.
E-mail: jmatt@uci.edu

DOI: 10.1175/2011JCLI4216.1

Atlantic sector, an order of magnitude greater than variations in total heat flux over the open ocean (Deser et al. 2000).

Sea ice–atmosphere interactions in the Pacific sector have been the focus of several studies. Using monthly averaged sea ice extent and cyclone frequency data for years 1958–80, Overland and Pease (1982) noted that Bering Sea sea ice extent was linked to wintertime storm-track location, which in turn is governed by the steering of cyclones by large-scale climate patterns, such as the WP. The relationship between Pacific sea ice and the WP pattern was then explicitly studied by Rogers (1981) using end-of-February sea ice concentrations for years 1968–77. Rogers (1981) found that Bering Sea sea ice advanced farther south in years when a trough in geopotential height over Alaska and the Aleutian Islands was deeper and farther east relative to its climatology, behavior associated with the positive polarity of the WP. This relationship was also observed by Cavalieri and Parkinson (1987) using daily sea ice extent data in winters between December 1972 and April 1976. Rogers (1981) reported an opposite response in the Sea of Okhotsk, where deepening of the Alaska–Aleutian trough associated with the positive WP coincided with retreating sea ice cover, though the signal was not as strong as that of Bering Sea sea ice.

In a more recent study using monthly average data in the period January 1979–December 2001, Linkin and Nigam (2008) found that the correlation between increased sea ice concentrations and the positive WP was only evident in the western Bering Sea. Furthermore, Linkin and Nigam (2008) found that the advance of sea ice in the Sea of Okhotsk was also associated with the positive WP, contrary to the findings of Rogers (1981) and Cavalieri and Parkinson (1987). Local variation in sea ice–atmosphere interactions in the Bering Sea was also studied by Sasaki and Minobe (2005) using a method of single-value decomposition on monthly averaged data for December–May in years 1870–2003. They found that sea ice variability in the northeastern Bering Sea between December and February was associated with a deepening of the Alaskan–Aleutian trough in geopotential height (the northward node of the WP), with similar findings for northwestern Bering Sea sea ice between March and May.

A limitation common to many of these studies is that they examine sea ice–atmosphere interaction using monthly or annually averaged data, which is problematic considering the short time scale of the WP (Feldstein 2000). This limitation is directly addressed by Linkin and Nigam (2008), who point out the need for weekly or shorter data averaging when dealing with sea ice–atmosphere interactions involving the WP. One recent study using observed weekly data to investigate the relationship between sea ice and atmospheric variability in the Atlantic sector is that of Strong et al. (2009). Using a linear stochastic model, Strong et al. (2009) tested directions of causality between the NAO and a dipole pattern in sea ice variability consisting of opposite-signed sea ice concentration anomalies in the Labrador and Barents Seas. One advantage of this approach is that feedback between sea ice and the atmosphere, which might otherwise be difficult to measure, can be readily deduced. In particular, Strong et al. (2009) found negative feedback between the NAO and the Labrador–Barents sea ice dipole, thus confirming the sign of feedback found in the modeling study of Magnusdottir et al. (2004).

Here, we investigate the observed relationship between Pacific sector patterns of sea ice concentration anomalies and the WP pattern on weekly time scales for Northern Hemisphere winters between 1979 and 2008. We, again, note that working on weekly time scales is essential if one is to accurately capture intraseasonal variability associated with the WP. We particularly focus on the existence and nature of feedback mechanisms, and draw comparisons with similar behavior in the Atlantic sector. Understanding the implications of possible future climate scenarios relies in part on understanding these feedback mechanisms. For example, should significant feedback between Pacific sea ice and the WP exist, how will the behavior of the WP and its associated climate effects change should sea ice decline and this feedback vanish?

The manuscript will proceed as follows: In section 2 we introduce observational data used in the study and the methodology used to process these data. This section also introduces the linear stochastic model used to analyze the relationship between sea ice and the WP pattern. Section 3a introduces patterns of sea ice and atmospheric variability, which are used in this study. Sections 3b and 3c examine observed coupling between sea ice anomalies and the atmosphere, motivating our choice of climate patterns used in the linear stochastic model. Feedback and causality are then studied in section 3d using this linear stochastic model. We summarize our findings in section 4a, and compare and contrast our results in the Pacific sector with those of Strong et al. (2009) for the Atlantic sector in section 4b.

2. Data and methodology

a. Datasets

Sea ice concentration data were taken from the National Snow and Ice Data Center (NSIDC) and are derived from *Nimbus-7* Scanning Multichannel Microwave

Radiometer and Defense Meteorological Satellite Program Special Sensor Microwave Imager radiances (Cavalieri et al. 2008). Geopotential height data were taken from the National Centers for Environmental Prediction–National Center for Atmospheric Research (NCEP–NCAR) reanalysis dataset. Sea ice data are available every two days from 1978 to 1986 and then once daily from 1987 to 2008. The winter season in 1987/88 is omitted in all analyses involving sea ice because of missing data between 3 December 1987 and 13 January 1988.

The winter period is defined as being the 21-week period with the first week starting 4 December and the final week starting 23 April. The linear trend over the period 1979–2008 is removed from the data, and the data are deseasonalized by removing the 1979–2008 weekly mean from each week in turn. Weekly averaging is performed starting 9 October and ending 6 June each year to accommodate lag correlation analysis.

b. Indices

Leading patterns of variability in sea ice and geopotential height are identified using empirical orthogonal function (EOF) analysis on the detrended and deseasonalized 21-week winter data for all winters. When studying sea ice variability, the analysis is restricted to the North Pacific region (30°–90°N, 90°W–90°E). For geopotential height data, EOFs are calculated at latitudes 25°–85°N using all longitudes, with the leading 19 modes of the EOF then being rotated using the varimax method (Kaiser 1958). This rotation reduces variances when projecting observed data onto the rotated modes, hence improving the relationship between these modes and physical teleconnection patterns compared to the unrotated modes. This avoids resorting to higher-order unrotated EOF modes when defining the WP. Principle components, referred to as indices from here on, are generated by projecting either sea ice concentration or geopotential height fields onto these EOFs, or selected portions thereof.

c. VAR model

The relationship between sea ice and the atmosphere, as represented by their respective indices B and W, is analyzed using a linear stochastic model (Enders 2004; Mosedale et al. 2006; Strong et al. 2009). Letting indices depend on their values at previous times requires expressing the model in vector form as a vector autoregressive [VAR(q)] model, where q is the maximum lag in the model. In the VAR(q) model framework, the indices at any given time, B_t and W_t, are related to their values at previous times by

$$\begin{pmatrix} B_t \\ W_t \end{pmatrix} = \sum_{i=1}^{q} \begin{pmatrix} a_i & b_i \\ c_i & d_i \end{pmatrix} \begin{pmatrix} B_{t-i} \\ W_{t-i} \end{pmatrix} + \begin{pmatrix} \epsilon_t^B \\ \epsilon_t^W \end{pmatrix}, \quad (1)$$

where $a_i, \ldots, d_i$ control the dependence of indices on their values in preceding weeks, and ϵ_t^B and ϵ_t^W are white-noise stochastic forcing terms representing random fluctuations in B and W, respectively.[1] The stochastic sequences ϵ_t^B and ϵ_t^W, which have distinct variances σ_B^2 and σ_W^2, are sometimes referred to as ''shocks,'' given that they perturb the purely autoregressive model by a random amount at each time. In the absence of these shocks, the indices would eventually decay to their long-term mean values, which in the case of deseasonalized and detrended data is $B_t = W_t = 0$ as $t \to \infty$. The VAR(q) model parameters $a_i, \ldots, d_i$, σ_B^2, and σ_W^2 are estimated by fitting (1) to observed B and W time series, as described in appendix A.

To identify which lagged dependencies in (1) significantly improve its capacity to model observed data, we investigate directions of Granger causality (Granger 1979). If index B Granger causes index W (denoted $B \Rightarrow W$), then knowledge of previous values of B improves predictions of W compared with knowledge of previous values of W alone; that is, a VAR(q) model with a lagged dependence of W on B is a significantly better fit to observed data than a model in which this direction of coupling is restricted. When testing for this relative improvement in model performance, we introduce the test statistic L given by

$$L = (T - n)(\log|\Sigma_r| - \log|\Sigma_u|), \quad (2)$$

where T is the number of weekly observations, $|\sum|$ is the determinant of the covariance matrix of residual errors in either the restricted (subscript r) or unrestricted model (subscript u), and n is the number of parameters $a_i, \ldots, d_i$ estimated in the unrestricted model (Sims 1980; Enders 2004). The test statistic L has an asymptotic χ^2 distribution in which the degrees of freedom are equal to the number of restrictions imposed when moving from the unrestricted to restricted model, or alternatively, the number of additional parameters in the unrestricted model compared to the restricted. When testing for significance, the null hypothesis H_0 assumes the restricted model is sufficient to describe the system. Rejection of H_0 implies that the restricted model is insufficient, with de facto acceptance of the unrestricted model as an alternative.

[1] Note that we use B_t or W_t when referring to specific weekly observations and B or W when referring to the index time series in general.

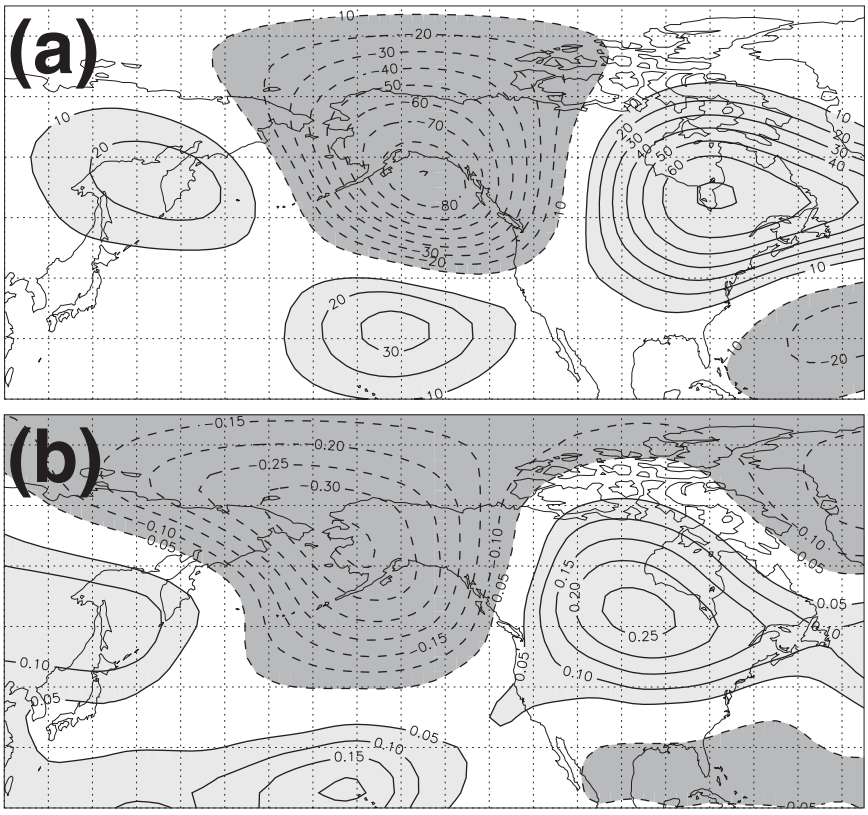

FIG. 1. (a) Leading rotated EOF of 500-hPa geopotential height anomalies, defining the WP teleconnection pattern. Contour interval is 10 m, with dark shading and dashed contours denoting negative anomalies. (b) Contemporaneous correlation of Bering Sea sea ice index B and 500-hPa geopotential height. Contour interval is 0.05, with dark shading and dashed contours denoting negative correlation.

We point out that as the number of estimated parameters in the VAR(q) model increases, the determinant of the covariance matrix of its residual errors will decrease. Therefore, as the unrestricted model estimates more parameters than the restricted model, it will always satisfy $\log|\sum_u| < \log|\sum_r|$, such that $L > 0$. Setting the degrees of freedom equal to the number of extra parameters in the unrestricted model when testing L for significance, as outlined above, offsets this improvement in model performance, ensuring that we only include parameters that offer *significant* improvement in model fit, thereby avoiding overparameterization.

3. Results

a. EOF analysis

Figure 1a shows the leading rotated EOF of geopotential height on the 500-hPa pressure surface in the Pacific–North American sector, which is closely associated with the WP teleconnection pattern. The WP here is characterized by a tripole pattern in geopotential height variability; the strongest center of action is a deep trough in geopotential height over Alaska, with positive centers of action over eastern Canada and the central Pacific north of Hawaii. This WP pattern is shifted westward when compared to that seen in some earlier studies (e.g., Wallace and Gutzler 1981), although good agreement exists between the WP shown here and that described by Nigam (2003). A thorough examination of this apparent shift in the WP constitutes a study in itself and is omitted here, although it is noted that a change in the characteristics of the WP may well affect its interaction with sea ice. In the remainder of the study, this pattern of atmospheric variability is used to define the WP and its associated index W.

Figures 2a and 2b show the leading two EOFs describing Pacific sector sea ice concentration variability on weekly time scales. The EOFs are distinct from one another (and higher-order EOFs) following the criterion of North et al. (1982) and describe 22% and 13% of the overall variability, respectively, with the next highest

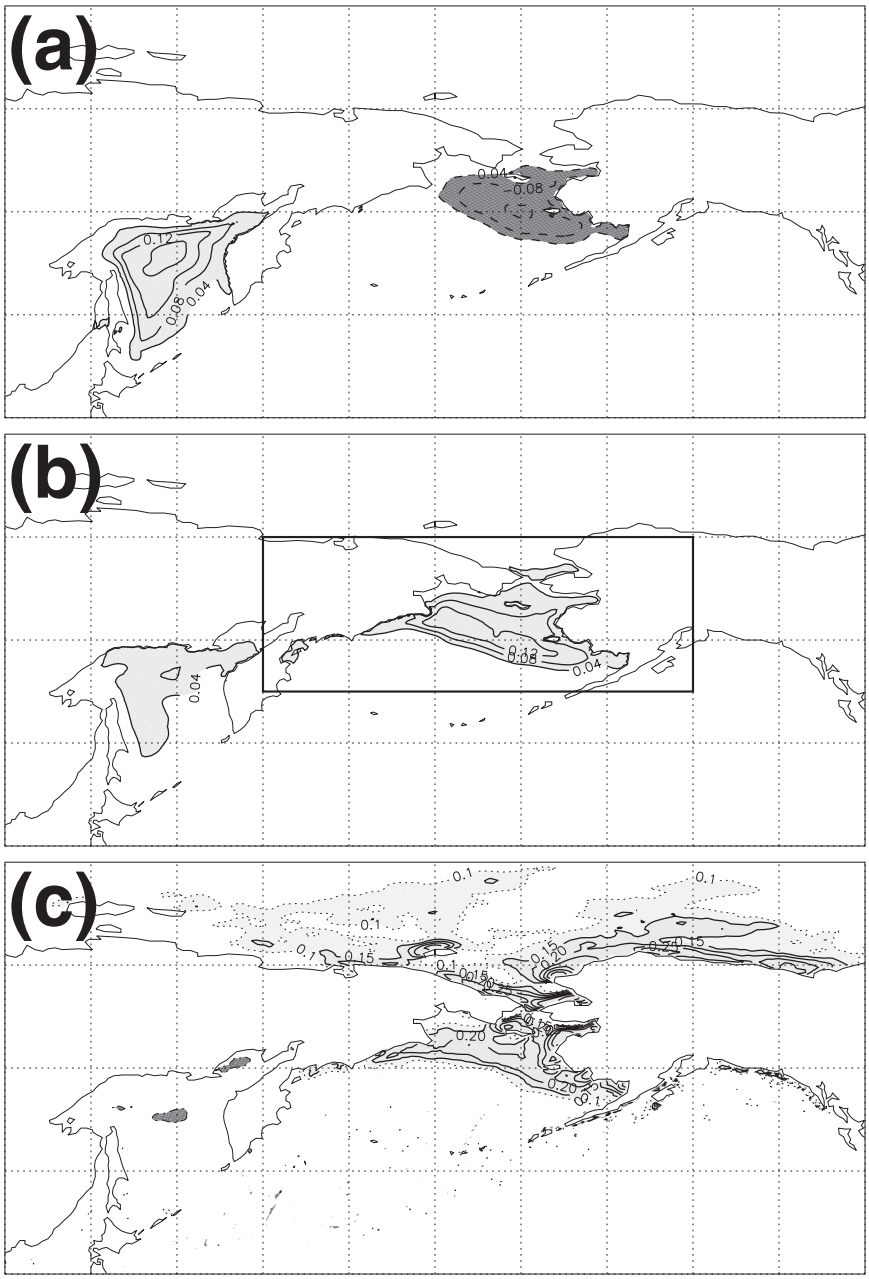

FIG. 2. (a) Leading EOF of sea ice concentration variability in the Pacific sector. Units are the fraction of area covered by sea ice. Contour interval is 0.04, with dark shading and dashed contours denoting negative anomalies. (b) As in (a), but for the second EOF. The local pattern used to generate the Bering Sea sea ice index B is marked by the rectangle. (c) Contemporaneous correlation between WP index W and sea ice concentration. Contour interval is 0.05, with dark shading and dashed contours denoting negative correlation. For visual aid, the 0.1 contour is dotted rather than solid.

mode describing 6% of the overall variability. The leading EOF is characterized by a dipole pattern, with centers of action over the Sea of Okhotsk and Bering Sea, as shown in Fig. 2a. This pattern is reminiscent of the Labrador–Barents dipole, which dominates sea ice variability in the North Atlantic (Deser et al. 2000), with a similar share of the overall variability (22% in the North Pacific in comparison to 20% in the North Atlantic). In contrast to this dipole pattern, the second EOF represents an in-phase advance or retreat of sea ice

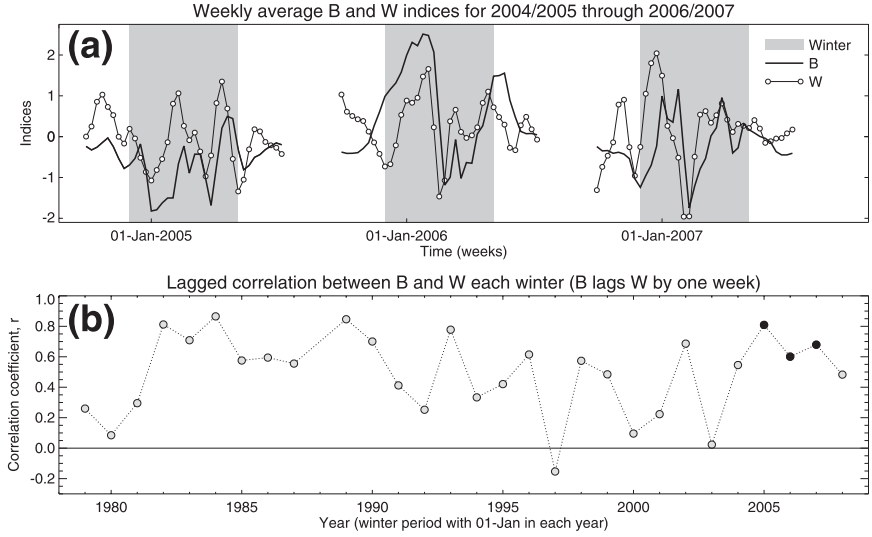

FIG. 3. (a) Weekly *B* (thick solid line) and *W* (thin solid line, circles) indices for winters with 1 Jan in years 2005–07, as indicated. Winter period of 21 weeks starting 4 December each year is marked by gray shading. (b) Lagged correlation between indices *W* and *B* over the 21-week winter period in each year, with *W* leading *B* by 1 week. Yearly markers correspond to winters including 1 Jan of that particular year. Black circles mark years shown in (a).

across both the Okhotsk and Bering Seas, with greater amplitude in the Bering Sea (Fig. 2b). Although a similar pattern is observed in the second EOF of North Atlantic sea ice variability, it is noted that its share of the overall variability is approximately half that observed here, and it is not well separated from higher-order EOFs; that is, sea ice variability in the Pacific sector is dominated by two modes of variability in contrast to the single dipole mode dominating the Atlantic sector.

b. Correlation analysis

At least one previous study (Liu et al. 2007) has found that sea ice anomalies in the Bering Sea and Sea of Okhotsk may be in phase just as often as they are out of phase, despite the dipole nature of the leading EOF seen in Fig. 2a. Therefore, it is useful to investigate whether the dynamical relationship of sea ice with the WP pattern is more prominent in one sea when compared to the other. Figure 2c shows the correlation of sea ice concentration anomalies with the WP pattern index *W* for the 21-week winter period. The largest positive correlation is observed in the Bering Sea and the neighboring Arctic Ocean, peaking at approximately 0.45 in the region of the Bering Strait. In contrast, the correlation between *W* and sea ice concentration in the Sea of Okhotsk is of order $O(10^{-2})$, suggesting that sea ice in this region is insensitive to changes in strength of the WP pattern. This indicates that on weekly time scales, the relationship between the WP teleconnection pattern and Pacific sea ice concentration is only noticeable in and around the Bering Sea. Therefore, for the remainder of this study, we focus on sea ice variability in the Bering Sea when investigating forcing and feedback between sea ice and the WP pattern. A corresponding index, *B*, is derived by projecting weekly sea ice concentrations onto the pattern shown within the rectangle in Fig. 2b, that is, the region (55°–70°N, 160°E–150°W).

The correlation between the Bering Sea sea ice index *B* and geopotential height on 500 hPa for the 21-week winter period is shown in Fig. 1b. The large negative correlation over Alaska indicates that in this region, changes in geopotential height coincide with changes in *B* of the opposite sign; that is, as the geopotential height anomaly becomes increasingly negative over Alaska, index *B* becomes increasingly positive, corresponding to an advance of the ice pack in the Bering Sea. Similarly, increasing geopotential height anomalies over Canada and the central Pacific Ocean also coincide with an increase in *B* because of the positive correlation in these regions. Comparison with Fig. 1a shows that the spatial structure of this correlation pattern is highly reminiscent of the WP pattern. This suggests that positive *W*, indicating deepening negative geopotential height anomalies over Alaska and increasing positive anomalies over Canada and the central Pacific, coincides with positive *B*, and vice versa for negative *W* and *B*.

This relationship between *W* and *B* can be observed directly in their weekly time series, as shown in Fig. 3a for winter in years 2004/05 and 2006/07. Fluctuations occurring on time scales of 4 weeks or less are damped in

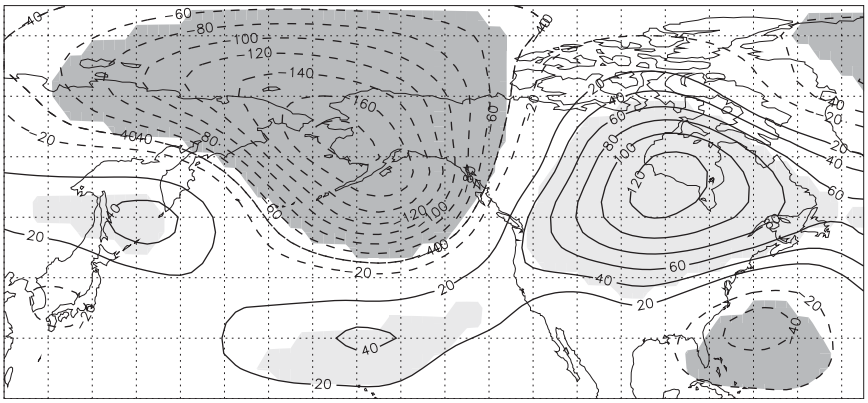

FIG. 4. Difference in composite geopotential height response between large positive/negative *B*. Contours are at intervals of 20 m, with negative contours dashed. Shading denotes regions in which the difference in response is significant at the 95% confidence level using a local *t* test.

W by applying a Butterworth filter (Butterworth 1930; Raymond and Gardner 1991). Overall, the indices follow one another closely, especially during the 21-week winter period. The correlation between *B* and *W* in each year is shown in Fig. 3b. When calculating the correlation, we use weeks within the 21-week winter period and let *B* lag *W* by one week, as this corresponds to the greatest correlation between the two indices, indicating that WP forcing of sea ice variability is the dominant process. However, contemporaneous correlation gives results similar to those shown here. All years but one exhibit positive correlation between *W* and *B*, with approximately 55% (16 out of 29) having a correlation coefficient greater than 0.5.

c. *Composite atmospheric response during extreme B regimes*

In addition to the correlation analysis described in the previous section, it is useful to observe geopotential height anomalies coinciding with large positive and negative values of *B*. Extreme values of index *B* are selected by locating local maxima and minima over all winters and then choosing the 29 largest such occurrences, giving approximately one extreme positive and negative event per year. The 500-hPa geopotential height response between extreme positive and negative *B* is then derived by subtracting the composite 500-hPa geopotential height for large negative *B* from that for positive *B*. Contours of the response are shown in Fig. 4 and show a pattern similar to that of the WP pattern seen in Fig. 1a, with a large negative response (exceeding $\pm$120 m) over the Bering Sea, Alaska, and northeast Siberia, and a large positive response over North America. A *t* test assuming local independence at each grid point indicates that this response is significant at the 95% confidence level in regions that are shaded. Note that the significant response is coincident with locations of high correlation in Fig. 1b. Most importantly, the magnitude of the composite response, which exceeds $\pm$120 m in the negative and positive centers of action over Alaska and Canada, respectively, shows that atmospheric anomalies associated with Bering Sea sea ice variability are noticeably large as well as being statistically significant.

d. *VAR(q) model results*

Although the correlation and composite response analyses suggest a relationship between Bering Sea sea ice concentrations and the WP pattern, seen in Fig. 1a, it is difficult to draw conclusions regarding causality. For example, it is difficult to tell to what extent changes in sea ice drive changes in the strength of the WP. As Honda et al. (1999) note, the atmospheric signal forced by sea ice anomalies may be disguised by the very same atmospheric anomalies that give rise to the sea ice anomalies in the first place. One strength of the VAR(q) model described in section 2c is its ability to isolate directions of causality, and by using it to examine feedback and causality between the WP pattern and Bering Sea sea ice concentrations, we now show that the WP forces like-signed changes in Bering Sea sea ice concentrations, which then exert a positive feedback onto the WP pattern.

For our unrestricted model U, we use the VAR(q) model with dependence in both directions. We then consider two variations of the restricted model: R1, where dependence of *W* on *B* is eliminated ($c_i \equiv 0$); and R2, where dependence of *B* on *W* is eliminated ($b_i \equiv 0$). For each model variation, the system in (1) is fit to the observed *B* and *W* weekly time series using ''seemingly unrelated regression'' (Zellner 1962), retrieving estimated

values for parameters $a_i, \ldots, d_i$ (see appendix A for further details).

One particular factor in VAR(q) model design is the choice of maximum lag q. Ideally, the lag should be long enough to include the most important dependencies between indices, while avoiding excess terms and overparameterization of the model. Inspection of the autocorrelation function for W and B shown in Fig. 5a suggests that the decorrelation of W occurs on time scales of 1–2 weeks, whereas the decorrelation of B occurs on longer time scales, typically 4–6 weeks. Figure 5b shows the partial autocorrelation functions for W and B, indicating the amount of autocorrelation that is not accounted for by lower lags (see appendix B for further details). At the 95% confidence level, contributions to the autocorrelation function at lags of 3 weeks or less are significant for both W and B, indicating that the smallest choice for q should be at least 3 weeks. Further consideration of Schwarz's criterion (Schwarz 1978; Enders 2004; Mosedale et al. 2006), Akaike's information criterion (Akaike 1974; Enders 2004), and a VAR(q)-based criterion [i.e., testing for significant improvement between models VAR(q_1) and VAR(q_2), see Enders (2004); Strong et al. (2009)] suggests an optimal lag of between 2 and 5 weeks, depending on how improvement in model performance is penalized by the inclusion of longer lags in each criterion. We therefore choose a maximum lag of $q = 4$ for our VAR(q) model to best accommodate these criteria. A physical interpretation of this choice is that Bering Sea sea ice concentrations and the WP only depend on their previous values and associated characteristics over the preceding 4 weeks, characteristics such as surface wind forcing and variation in heat flux from the ocean to the atmosphere. Note that the time scale of this dependence is shorter than the monthly time scales considered in previous studies.

Comparing the VAR(4) unrestricted model with each of the restricted models in turn gives test statistics of $L = 15.00$ when comparing models U and R1 (W independent of B) and $L = 62.56$ when comparing models U and R2 (B independent of W).[2] In both cases, we reject the null hypothesis at the 95% confidence level with reference statistic $t = 9.49$, setting our degrees of freedom equal to 4 given the four restrictions imposed by setting $c_i \equiv 0$ and $b_i \equiv 0$ for $1 \leq i \leq 4$ in R1 and R2, respectively; that is, Granger causality exists in both directions $B \Leftrightarrow W$, and the VAR(4) model, including lagged dependence of B and W on one another, is significantly better at modeling observed data than a model in which either direction of causality is restricted.

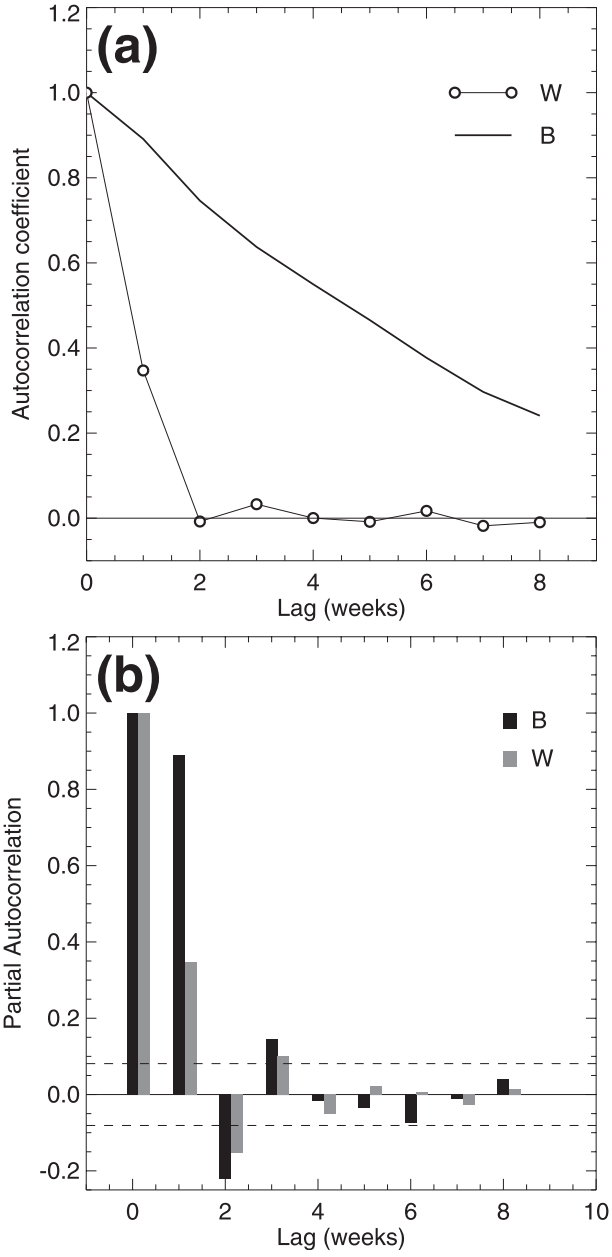

FIG. 5. (a) Autocorrelation of B (thick line) and W (thin line, circles) as a function of time (weeks). (b) Partial autocorrelation of B (black) and W (gray) as a function of time. Dashed line marks the approximate 95% confidence limit at $\pm 2/\sqrt{T}$, where $T = 609$ is the total number of observations over all 21-week winter periods.

Parameters $a_i, \ldots, d_i$ for the unrestricted VAR(4) model U, calculated by fitting model U to the observed B and W time series as outlined in appendix A, are shown in Table 1. Interaction between lagged terms

[2] Test statistic L defined in Eq. (2), using $T = 609$ weekly observations and estimating $n = 16$ parameters $a_i, \ldots, d_i$ in the unrestricted model U.

TABLE 1. VAR(4) parameters for model U.

i	1	2	3	4
a_i	1.01	−0.12	−0.08	0.09
b_i	0.16	−0.17	0.09	−0.04
c_i	−0.26	0.35	−0.35	0.27
d_i	0.48	−0.23	0.17	−0.07

TABLE 2. VAR(4) parameters for model R1.

i	1	2	3	4
a_i	1.08	−0.22	0.02	0.02
b_i	0.14	−0.16	0.08	−0.04
c_i	0.00	0.00	0.00	0.00
d_i	0.40	−0.20	0.13	−0.07

makes direct interpretation of the values of $a_i, \ldots, d_i$ difficult. Therefore, to measure the feedback of sea ice onto the WP, we perform two experiments using the VAR(4) model with, and without, the dependence of W on B. The first experiment uses the unrestricted VAR(4) model U, in which B and W both depend on the previous values of one another. The second experiment uses the restricted VAR(4) model R1, in which W is independent of previous B values. The parameters $a_i, \ldots, d_i$ for each experiment are given in Table 1 (experiment U) and Table 2 (experiment R1, where $c_i \equiv 0$) and are obtained by fitting the appropriate model (U or R1) to observed data as outlined in appendix A. To differentiate between these experiments, indices in experiment R1 where feedback from sea ice is removed are labeled B^* and W^*, whereas indices in the fully coupled model U are labeled B and W. In each experiment, index values at times $-4 \le t \le 0$ are derived by compositing each index around times at which B is large and positive, that is, the 29 extreme positive B times used in section 3c. Index values at times $t > 0$ are generated by advancing the equations in (1) with time. Because the white-noise stochastic forcing in (1) has zero mean, taking an ensemble mean of many stochastically forced model outcomes is equivalent to setting $\epsilon_t^B = \epsilon_t^W = 0$ in (1) and performing a single deterministic model realization with the appropriate model parameters $a_i, \ldots, d_i$. Because both models U and R1 are stable, index values will decay to zero as time increases, as described in section 2c. This can be interpreted as the individual stochastic model outcomes becoming increasing uncorrelated with one another at large times, such that their ensemble mean decays to zero. The role of feedback can be determined by investigating how this decay differs between models U and R1.

Figure 6 shows model experiments for VAR(4) with (solid lines), and without (dashed lines), feedback of Bering Sea sea ice onto the WP. In general, feedback from B onto W would be observed as follows for either negative or positive feedback:

- In the case of negative feedback from B onto W, initially large B values will damp W as time progresses, such that W in the model with feedback decays faster than W^* in the model without feedback. As positive W forces positive B (because of their positive correlation, as described in section 3b), smaller W means B will decay faster in the model with feedback when compared to B^* in the model without feedback.
- In the case of positive feedback from B onto W, the opposite will be true. Initially large B values will sustain positive W as time progresses, such that W in the model with feedback decays slower than W^* in the model without feedback. Because of positive W forcing positive B, we then expect positive B values to be sustained when compared to B^*.

Following this description, in Fig. 6 we see a positive feedback mechanism between B and W in the VAR(4) model. When W^* is independent of B^*, W^* quickly returns to zero at lags greater than 2 weeks, which is to be expected, given its naturally short decorrelation time scale of approximately 1 week (seen in Fig. 5a). However, when looking at W and B in the fully coupled model with feedback, dependence on B acts to increase W at lags greater than 3 weeks. This increase in W,

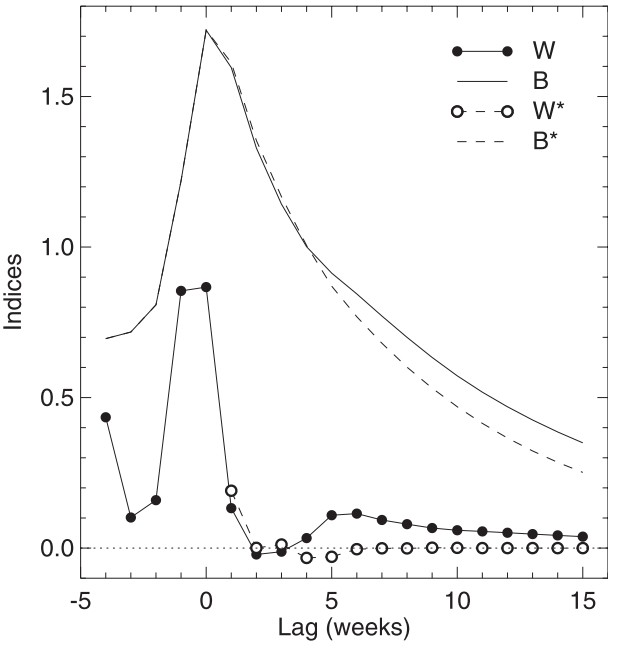

FIG. 6. Comparison in VAR(4) model behavior when including feedback of B onto W (solid line with and without symbols) and excluding feedback (B^*, W^*, dashed line with and without symbols).

relative to W^*, peaks at a lag of 6 weeks before W slowly decays back to zero. Feedback of increased W values onto B then acts to sustain high values of B as described above, in turn sustaining increased values of W.

It is notable that this positive feedback is perhaps counterintuitive when looking directly at the parameters in Table 1, where the negative sign of parameter c_1 may suggest a negative feedback of B onto W. This goes to show that one must be careful when directly interpreting the values of parameters $a_i, \ldots, d_i$.

4. Discussion

a. Bering Sea sea ice interaction with the WP pattern

This study has focused on the interaction between atmospheric and sea ice variability in the Pacific sector during Northern Hemisphere winter. Because of the short time scale of atmospheric variability in this region, we use weekly averaged data in the period 1978–2008, rather than monthly or annually averaged data (e.g., Liu et al. 2007; Linkin and Nigam 2008; Sasaki and Minobe 2005).

The WP pattern, objectively defined using the leading rotated EOF in 500-hPa geopotential height, was chosen as a measure of atmospheric variability in the Pacific sector. Correlation analysis using the weekly WP index shows that changes in sea ice concentration associated with the WP are confined to the Bering Sea, with almost no response in the Sea of Okhotsk, as shown in Fig. 2c. When the WP is in its positive polarity, corresponding to a deepening trough in geopotential height over Alaska, sea ice concentrations increase in the Bering Sea. Similarly, the negative polarity of the WP is accompanied by decreased sea ice concentrations in the Bering Sea. The strongest correlation between Bering Sea sea ice concentrations and the WP occurs when sea ice lags the WP by one week, suggesting that atmospheric forcing of sea ice is the dominant mechanism linking the two, a finding that is consistent with existing studies. Previous studies have remarked on the difficulty in directly measuring the feedback of sea ice back onto the atmosphere (e.g., Honda et al. 1999) because the atmospheric anomalies forcing changes in sea ice can mask the feedback signal. However, by fitting a linear stochastic model to the observed weekly data, a positive feedback mechanism is identified between Bering Sea sea ice and the WP pattern; that is, positive WP leads to increasing Bering Sea sea ice concentrations, which then sustain the positive WP via feedback, as shown in Fig. 6. A similar relationship holds for negative WP and decreasing Bering Sea sea ice concentrations. In both cases, these sustained atmospheric forcing conditions lead to sustained anomalies in Bering Sea sea ice concentrations. The positive feedback of Bering Sea sea ice onto the atmosphere, detected here using observed data, supports the sign of feedback found in the modeling study of Alexander et al. (2004). We note that while changes in sea ice in the Sea of Okhotsk do not exert significant feedback onto the WP, feedback mechanisms may exist between more local patterns of atmospheric variability, although a thorough examination of this possibility is for future study.

The forcing and feedback relationship between the WP and Bering Sea sea ice indices can be understood in terms of the physical mechanisms they represent. Regimes of large positive WP index are characterized by strong northerly winds over the Bering Sea that advect sea ice away from the coast, thus boosting sea ice concentrations and leading to large positive Bering Sea sea ice index. The opposite is true in regimes where the WP index is large and negative; weaker northerly winds mean less ice is advected away from the coast, leading to reduced ice concentrations throughout the Bering Sea and negative values for the Bering Sea sea ice index. These variations in sea ice concentrations then exert feedback by changing sensible and latent heat fluxes from the ocean to the atmosphere.

b. Comparisons with the North Atlantic sector

Strong et al. (2009) studied the observed feedback between the Greenland sea ice dipole (a dipole in sea ice concentrations between the Barents and Labrador Seas) and the NAO on weekly time scales using a stochastically forced VAR model similar to that described in section 2c. The NAO and WP have similar features: both are characterized by a seesaw in 500-hPa geopotential height over the Atlantic and Pacific Oceans, respectively (with an additional center of action over North America in the case of the WP, as seen in Fig. 1a), and both are important drivers of regional climate variability. Sea ice variability in the Pacific also shows similarity with sea ice variability in the Atlantic. In both sectors, the leading mode of variability appears as a dipole in sea ice concentration, between the Barents and Labrador Seas in the Atlantic sector, and the Sea of Okhotsk and the Bering Sea in the Pacific sector (Deser et al. 2000; Liu et al. 2007; Ukita et al. 2007; Fig. 2a). However, coastal boundaries are entirely different between the two basins, as is the latitudinal extent of sea ice. Typically, sea ice in the Atlantic sector does not extend as far south as sea ice in the Pacific sector, partly because an important difference in the ocean circulation: poleward transport of heat toward the Barents Sea occurs via the North Atlantic Drift, whereas there is relatively little poleward transport of heat into the Sea of Okhotsk and Bering Sea by the North Pacific Drift. One further difference is in

the location of storm tracks, with the North Atlantic storm track remaining close to the marginal ice zone compared to the North Pacific storm track.

The way in which the atmosphere interacts with sea ice in each sector is quite different. In contrast to the Atlantic sector, where the NAO forces a dipole in sea ice concentration anomalies, the Pacific sea ice response to the WP is only noticeable in the Bering Sea (cf. Figure 2c), and it does not project onto the leading dipole mode of sea ice concentration variability.

There is also an important difference in the way changes in sea ice feed back onto the atmosphere. In their study, Strong et al. (2009) found a negative feedback of sea ice onto the atmosphere, such that NAO-forced sea ice anomalies damped the initial forcing conditions. Here, the opposite is found in the Pacific sector, with a positive feedback existing between Bering Sea sea ice and the WP. This positive feedback means that Bering Sea sea ice helps sustain large positive or negative WP conditions (cf. Figure 6), thereby lengthening the WP's time scale of variability.

The existence of this positive feedback mechanism enables us to speculate on the role of Pacific sea ice in future climate scenarios. In scenarios where the Bering Sea is mostly free of sea ice during the winter, one might expect increased variability in the WP because of the absence of sea ice and its associated positive feedback. Conversely, climate scenarios with increased wintertime Bering Sea sea ice concentrations may exhibit a less erratic WP because positive feedback from sea ice helps sustain preexisting WP conditions. These possible changes in WP variability would play an important role when considering climate features associated with the WP, such as North American precipitation patterns.

Acknowledgments. This work was supported by NOAA Grant NA09OAR4310132. The authors thank Hal Stern and Court Strong for their helpful suggestions concerning the implementation of the VAR model framework, and three anonymous reviewers for their helpful comments on the manuscript.

APPENDIX A

Estimating Parameters of the VAR(q) Model

The VAR(q) model parameters a_i, b_i, c_i, and d_i are estimated by fitting (1) to observed B_t and W_t time series, with residual errors (e_t^B, e_t^W) replacing stochastic forcing terms $(\epsilon_t^B, \epsilon_t^W)$. When fitting the model, the left-hand side of (1) uses B_t and W_t values in the 21-week winter period each year, with weeks before 4 December being used for lagged values on the right-hand side where necessary. The remaining two unknown parameters in the system, variances σ_B^2 and σ_W^2 of the stochastic forcing terms, are given by the following covariance matrix of these residual error terms:

$$\sum = \begin{pmatrix} \mathrm{var}(e_t^B) & \mathrm{cov}(e_t^B, e_t^W) \\ \mathrm{cov}(e_t^B, e_t^W) & \mathrm{var}(e_t^W) \end{pmatrix}, \tag{A1}$$

where $\sigma_B^2 = \mathrm{var}(\epsilon_t^B) = \mathrm{var}(e_t^B)$ and $\sigma_W^2 = \mathrm{var}(\epsilon_t^W) = \mathrm{var}(e_t^W)$.

As we impose asymmetrical restrictions on these lagged dependencies (e.g., $c_i \equiv 0$ in model R1 of section 3d, meaning B depends on both B and W, whereas W depends only on itself), it is statistically efficient to fit the model to observed data using seemingly unrelated regression (SUR) rather than ordinary least squares regression (OLS) (Zellner 1962; Enders 2004). The SUR method is similar to that of OLS and is omitted here in the interest of brevity. However, we note that in cases where B_t and W_t have exactly the same number of lagged dependencies, parameter estimates using SUR and OLS are identical.

APPENDIX B

Coefficients of the Partial Autocorrelation Function

Coefficients in the partial correlation function are calculated using the "sweep" algorithm of Thisted (1988), which is summarized here for convenience. For any time series y_t with T observations, we construct matrix Y using

$$Y = \{y_{t-q}, y_{t-q+1}, \ldots, y_{t-1}, y_t\},$$

where q is the maximum lag and Y has dimension $T \times q$. A sum of squares and cross products matrix S is then constructed using

$$S = Y'Y,$$

where the prime denotes transposition and S has the dimension $q \times q$. We then define the sweep operator $\mathcal{L}$ such that

$$\tilde{S} = \mathcal{L}S,$$

where elements $\{\tilde{s}_{ij}\}$ in $\tilde{S}$ are calculated from elements $\{s_{ij}\}$ in S using

$$\tilde{s}_{kk} = -\frac{1}{s_{kk}},$$

$$\tilde{s}_{ik} = -\frac{s_{ik}}{s_{kk}} \quad i \neq k,$$

$$\tilde{s}_{kj} = -\frac{s_{kj}}{s_{kk}} \quad j \neq k, \quad \text{and}$$

$$\tilde{s}_{ij} = s_{ij} - \frac{s_{ik}s_{kj}}{s_{kk}} \quad i \neq k \quad j \neq k.$$

Applying the sweep operator n times gives

$$\tilde{S}^{(n)} = \mathcal{L}\tilde{S}^{(n-1)} = \mathcal{L}^n S \quad 1 \leq n \leq q.$$

The elements of $\tilde{S}^{(n)}$ are interpreted as partial autoregression coefficients by writing

$$y_t = \tilde{s}_{n1}^{(n)} y_{t-1} + \tilde{s}_{n2}^{(n)} y_{t-2} + \cdots + \tilde{s}_{nn}^{(n)} y_{t-n} + \cdots + \tilde{s}_{nq}^{(n)} y_{t-q},$$

where $\tilde{s}_{nn}^{(n)}$ is the correlation between y_t and y_{t-n} when all cross correlations with intervening terms $y_{t-1}, \ldots, y_{t-n+1}$ have been removed. The partial autocorrelation function for lags 1 to q therefore takes values $(\tilde{s}_{11}^{(1)}, \tilde{s}_{22}^{(2)}, \ldots, \tilde{s}_{qq}^{(q)})$, as shown for B and W in Fig. 5b when $q = 8$.

REFERENCES

Akaike, H., 1974: A new look at the statistical model identification. *IEEE Trans. Autom. Control,* **19,** 716–723.

Alexander, M. A., U. S. Bhatt, J. E. Walsh, M. S. Timlin, J. S. Miller, and D. Scott, 2004: The atmospheric response to realistic Arctic sea ice anomalies in an AGCM during winter. *J. Climate,* **17,** 890–905.

Butterworth, S., 1930: Theory of filter amplifiers. *Exp. Wireless Wireless Eng.,* **7,** 536–541.

Cavalieri, D. J., and C. L. Parkinson, 1987: On the relationship between atmospheric circulation and the fluctuations in the sea ice extents of the Bering and Okhotsk Seas. *J. Geophys. Res.,* **92,** 7141–7162.

——, ——, P. Gloerson, and H. J. Zwally, 2008: Sea ice concentrations from Nimbus-7 SMMR and DMSP SSM/I passive microwave data, 1978–2008. National Snow and Ice Data Center, Boulder, CO, digital media. [Available online at http://nsidc.org/data/nsidc-0051.html.]

Deser, C., J. E. Walsh, and M. S. Timlin, 2000: Arctic sea ice variability in the context of recent atmospheric circulation trends. *J. Climate,* **13,** 617–633.

Enders, W., 2004: *Applied Econometric Time Series*. 2nd ed. Wiley, 466 pp.

Fang, Z., and J. M. Wallace, 1994: Arctic sea ice variability on a timescale of weeks and its relation to atmospheric forcing. *J. Climate,* **7,** 1897–1914.

Feldstein, S. B., 2000: The timescale, power spectra, and climate noise properties of teleconnection patterns. *J. Climate,* **13,** 4430–4440.

Granger, C. W. J., 1979: Investigating causal relationships by econometric models and cross spectral methods. *Econometrica,* **37,** 473–485.

Honda, M., E. Yamazaki, H. Nakamura, and K. Takeuchi, 1999: Dynamic and thermodynamic characteristics of atmospheric response to anomalous sea-ice extent in the Sea of Okhotsk. *J. Climate,* **12,** 3347–3358.

Kaiser, H. F., 1958: The varimax criterion for analytic rotation in factor analysis. *Psychometrika,* **23,** 187–200.

Linkin, M. E., and S. Nigam, 2008: The North Pacific Oscillation–west Pacific teleconnection pattern: Mature-phase structure and winter impacts. *J. Climate,* **21,** 1979–1997.

Liu, J., Z. Zhang, R. M. Horton, C. Wang, and X. Ren, 2007: Variability of North Pacific sea ice and East Asia–North Pacific winter climate. *J. Climate,* **20,** 1991–2001.

Magnusdottir, G., C. Deser, and R. Saravanan, 2004: The effects of North Atlantic SST and sea ice anomalies on the winter circulation in CCM3. Part I: Main features and storm track characteristics of the response. *J. Climate,* **17,** 857–876.

Mosedale, T. J., D. B. Stephenson, M. Collins, and T. C. Mills, 2006: Granger causality of coupled climate processes: Ocean feedback on the North Atlantic Oscillation. *J. Climate,* **19,** 1182–1194.

Nigam, S., 2003: Teleconnections. *Encyclopedia of Atmospheric Sciences,* J. R. Holton, J. A. Pyle, and J. A. Curry, Eds., Academic Press, 2243–2257.

North, G. R., T. L. Bell, R. F. Cahalan, and J. Moeng, 1982: Sampling errors in the estimation of empirical orthogonal functions. *Mon. Wea. Rev.,* **110,** 699–706.

Overland, J. E., and C. H. Pease, 1982: Cyclone climatology of the Bering Sea and its relation to sea ice extent. *Mon. Wea. Rev.,* **110,** 5–13.

Raymond, W. H., and A. Gardner, 1991: A review of recursive and implicit filters. *Mon. Wea. Rev.,* **119,** 477–495.

Rogers, J. C., 1981: The North Pacific Oscillation. *J. Climatol.,* **1,** 39–57.

Sasaki, Y. N., and S. Minobe, 2005: Seasonally dependent interannual variability of sea ice in the Bering Sea and its relation to atmospheric fluctuations. *J. Geophys. Res.,* **110,** C05011, doi:10.1029/2004JC002486.

Schwarz, G., 1978: Estimating the dimensions of a model. *Ann. Stat.,* **6,** 461–464.

Sims, C. A., 1980: Macroeconomics and reality. *Econometrica,* **48,** 1–48.

Strong, C., G. Magnusdottir, and H. Stern, 2009: Observed feedback between winter sea ice and the North Atlantic Oscillation. *J. Climate,* **22,** 6021–6032.

Thisted, R. A., 1988: *Elements of Statistical Computing*. 1st ed. Chapman and Hall, 427 pp.

Ukita, J., M. Honda, H. Nakamura, Y. Tachibana, D. J. Cavalieri, C. L. Parkinson, H. Koide, and K. Yamamoto, 2007: Northern Hemisphere sea ice variability: Lag structure and its implications. *Tellus,* **59A,** 261–272.

Walker, G. T., and E. W. Bliss, 1932: World weather V. *Mem. Roy. Meteor. Soc.,* **4,** 53–84.

Wallace, J. M., and D. S. Gutzler, 1981: Teleconnections in the geopotential height field during Northern Hemisphere winter. *Mon. Wea. Rev.,* **109,** 784–812.

Zellner, A., 1962: An efficient method of estimating seemingly unrelated regressions and tests for aggregation bias. *J. Amer. Stat. Assoc.,* **57,** 348–368.